Impact of C-CVD synthesis conditions on the hydraulic and electronic properties of SiC/CNTs nanocomposite microfiltration membranes

Alexandre Poli, Ghadi Dagher, Alexandre Ferreira Santos, Patrick Baldoni-Andrey, Matthieu Jacob, Catherine Batiot-Dupeyrat, Benoit Teychené

Impact of C-CVD synthesis conditions on the hydraulic and electronic properties of SiC/CNTs nanocomposite microfiltration membranes

Alexandre Poli [a], Ghadi Dagher [a], Alexandre Ferreira Santos [b], Patrick Baldoni-Andrey [c], Matthieu Jacob [c], Catherine Batiot-Dupeyrat [a], Benoit Teychene [a,*]

[a] IC2MP (UMR CNRS 7285), Universit´e de Poitiers, 1 rue Marcel Dor´e, 86000 Poitiers, France
[b] UFPR, 1299 Rua XV de Novembro, 80060-000 Curitiba, Brazil [c] TotalEnergies, PERL, Route de Bayonne, 64170 Lacq, France

ARTICLEINFO

Keywords:
SiC ceramic membrane
Carbon nanotubes
Hybrid membrane
Conductive membrane
CVD

ABSTRACT

In this study, commercial SiC ceramic microfiltration membranes were coated with carbon nanotubes (CNTs) using chemical vapor deposition (CVD) to obtain a conductive and hydrophobic membrane material. In order to have better control of the surface and electronic properties of the developed material, two adjacent fractional factorial designs (2^{5-2}) were implemented to quantify CNTs synthesis parameters influence. The design of experiments revealed that the quantity of the synthesized CNTs was mainly controlled by CVD temperature, duration and iron catalyst concentration. The structure of the CNTs layer was mainly controlled by CVD temperature within the investigated parameter range (650–850 °C). It was demonstrated that pure water permeability was anti-correlated with CNTs synthesis yield due to an increase in membranes' hydrophobicity and potential pore blockage. The membrane coated with the largest amount of CNTs was obtained at 850 °C for a duration of at least 1 h and showed relatively low electrical resistance and good microwave absorption. Finally, such tunable nanocomposite material has the potential to further improve the filtration performances and membranes widespread application.

1. Introduction

In recent years, a specific attention has been paid to ceramic membranes (inorganic materials) regarding industrial effluents treatment [1,2]. Despite their lower mechanical resistance, ceramic materials exhibit longer lifetimes due to their excellent chemical, thermal stability and their resistance towards harsh filtration conditions. However, membrane processes widespread application is still hindered by fouling phenomena [3]. One way to limit or control this phenomenon is to modify the surface properties of the membrane material [4]. As recently reviewed by Raji et al. [5], ceramic membrane surface functionalization was intensively explored and specifically aims to improve the wettability of the material. Controlling membrane surface properties in order to mitigate fouling is a complex task, as the wettability depends on many factors such as: roughness [6], chemical nature of the surface [7] or surface electrostatic charge [8]. Surfaces functionalization might be achieved by several physical and chemical methods including ion beam & plasma irradiation [9], vapor phase deposition [10], coating [11] and membrane grafting [12].

Fouling is also highly dependent on the feed conditions (pollutants concentration and nature) and its variability over time. Consequently, robust surface modification seems to be an adequate solution to perform efficient liquid solid separation [13,14]. Notably, the use of nanomaterials to develop composite inorganic membranes has the potential for further enhancing the filtration performances [15].

Despite their hydrophobicity, carbon nanotubes (CNTs) have raised a high interest due to their high aspect ratio [16–18] and their capability to be functionalized [19,20]. For example, Saththasivam et al. (2018) [21] created a membrane with CNTs functionalized with hydrophilic MnO_2 showing higher water flux compared to a pristine CNTs membrane and efficient towards oil in water emulsion (O/W) separation. An et al. (2018) [8] made a Janus membrane, suitable to treat both O/W and water in oil (W/O) emulsions. Roman-Manso et al. (2014) ´ [22] reported the fabrication of silicon carbide (SiC)/CNTs composite pillars through Chemical Vapor Deposition (CVD) process demonstrating superhydrophobic and superoleophilic (under-air) properties. Many other examples of CNTs modified membranes are available in literature, for applications in clean water production [23,24], desalination [24], air treatment or more general applications [25–30].

Only few articles reported the functionalization of ceramic membranes (MF or UF) through in situ growth of CNTs in order to functionalize membrane surface. Chen et al. (2012) [31] pioneered the design of a homemade mullite based ceramic/CNTs composite membrane via in situ growth of CNTs using CVD process (membrane surface area of 2 cm^2). Later Tran et al. (2015) [10] demonstrated the possibility to scale up the synthesis process (membrane surface area of 51 cm^2) onto tubular commercial ceramic membranes in Al_2O_3 by catalytic CVD (C- CVD). More recently, Yuan et al. (2020) [32] prepared a SiC-CNTs composite membrane for air treatment via in situ growth of CNTs by C-CVD. These recent articles suggested that the composite membrane efficiency is strongly related to the steric configuration of the synthesized CNTs (i.e.: nature and quantity) produced during the C-CVD procedure.

CVD synthesis parameters such as the catalyst type and size [33–39], substrate characteristics [40,41], nature of the carbon source [42–44], temperature [16,45–47] or gas hydrodynamic during CVD [28,48] and can be played on to obtain the desired CNTs structure and properties. [49].

More precisely, catalyst impregnation step is one of the most important features as the size of the catalyst particle is highly correlated to CNTs diameter [50] and its density at the material surface will impact nanotubes yield [51]. Catalyst morphology might not be directly controlled as it is the consequence of many other parameters such as: catalyst nature, dispersion method, calcination and reduction temperature [52].

In addition, the CVD parameters (temperature, duration, hydrocarbons, etc.) will be mainly responsible for the structure and length of the CNTs. For instance, a longer duration will let CNTs grow longer [53]. The hydrocarbon gas ratio will impact the electrical conductivity (i.e. the structure) of the CNTs [39]. Temperature seems to impact the diameter of nanotubes and their nature but reported results are contradictory. For example, Bulyarskiy et al. [53] found increasing CNTs diameter with temperature while Nourbakhsh et al. [54] found the opposite trend working in the same temperature range (700–800 °C).

This short literature review illustrates the difficulty to draw a general framework of CNTs growth by CVD as setups and synthesis conditions are often different. This is especially true for the specific case of CNTs growth on ceramic porous filtration membrane.

This articles aims at investigate the influence of the main CVD parameters on the properties of SiC/CNTs composite ceramic microfiltration membranes. Specifically, the presented study focus on the control of CNTs synthesis on

commercial SiC ceramic microfiltration membranes by working with a fractional factorial screening design of experiment (DoE). Five parameters influencing the CVD process were specifically studied: the concentration of catalyst (Fe) in the dip-coating solution, the hydrocarbon (C_2H_6) gas fraction in the gas blend during CVD, the calcination temperature, the CVD temperature and duration. The objectives are to identify the key parameters impacting the amount and quality of anchored carbon material synthesized at the membrane surface where the foulant interaction is expected to be the most important. Finally, the CVD parameters are linked to the composite membrane physico-chemical properties (surface wettability, filterability, electronic properties) that can be tuned to fit the required properties.

2. Material and methods

2.1. Membrane material

Flat sheet SiC membrane modules (0.175 m^2, L615 × W150 × T6/12 mm) were purchased from Cembrane company (Denmark). This membrane is fully made of SiC and presents a 60 µm thick active layer with a mean pore size of 0.1 µm supported on SiC (i.e. 90% removals of particles greater than 0.1 µm according to the manufacturer). For the DoE methodology, the commercial membranes were cut in L30 × W10 × T2 mm pieces (3 cm^2 active area, Fig. S1 of Supplementary data).

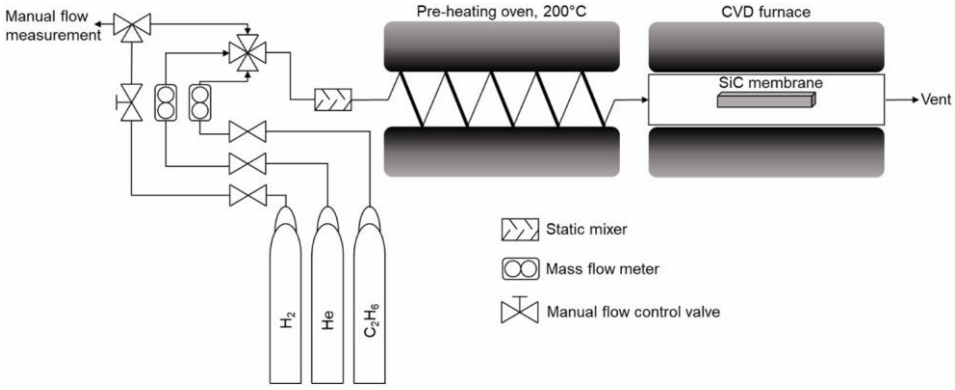

Fig. 1. Schematic representation of the CVD set-up.

For pure water permeability measurements, membranes were cut in larger pieces of 55 cm^2 filtration surface area (L145 × W30 × T6 mm initial pieces, Fig. S2 of Supplementary data) and operated on a lab-scale constant flux submerged filtration pilot (see Fig. S3 of Supplementary data).

Only relevant CVD synthesis conditions deducted from the DoE experiments were selected for scale up and material properties evaluation (pure water flux, wettability, electronic properties).

2.2. CNTs growth by Catalytic Chemical Vapor Deposition (C-CVD) and characterization

CNTs were grown on catalyst coated SiC membranes in a hot-wall horizontal chemical vapor reactor from conditions generated by the screening design (see Section 2.3). Every membrane sample was initially washed with deionized water, before being dried at 100 °C.

Iron based catalyst was deposited on the membranes by dip-coating - oxidation - reduction method [45]. Iron was preferred compared to other catalysts (Ni, Co…) as it was assumed to be more compatible with water treatment processes. Membranes were first soaked for 30 min in an ultrasonic bath (300 W at room temperature) filled with Fe^{3+} (0.5 to 2.5 wt% in Fe) solution prepared from $FeCl_3.6H_2O$ (Sigma-Aldrich). Impregnated membranes were then dried at 100 °C before calcination at temperatures ranged from 200 to 500 °C for 2 h.

Iron oxide coated membranes were afterward placed in the middle of the CVD quartz tube reactor (as shown in Fig. 1) under a 1:1 ratio He:H_2 mix (120 mL· min^{-1} total flow, Re ~ 4). Reactor was heated up to 600 °C for 1 h to reduce metal oxide to the active Fe(0) catalyst [10].

Subsequently, temperature was increased to the reaction temperature and gas inlet was switched to a He:C_2H_6 blend (120 mL· min^{-1} total flow) for the synthesis duration (30 to 90 min). After synthesis completion, gas inlet was set back to the initial 1:1 ratio He:H_2 mix until cooling down to room temperature. Ethane was chosen as it is a cheap and non-toxic gas compared to other gaseous sources. Also as previously reported ethane allows significant synthesis yield of carbon nanomaterials during CVD [55].

After synthesis all samples were immediately washed in MilliQ water in an Elmasonic S 30 H ultrasonic bath (300 W) per 30 min cycles (T < 40 °C) until nothing came out of the membrane. Finally all membranes were dried at 100 °C prior further use.

It is important to note that every analyzed sample undergone this ultrasonic cleaning procedure in order to investigate only well anchored CNTs and to avoid any potential CNTs leakage during filtration process.

The carbon material synthesis yield (C wt% yield) was determined in triplicate (Std Dev 2.2%) by thermal analysis (TGA/DSC) using a Q series Q600-0471 analyzer (TA Instruments, USA) after crushing samples into powder using a mortar. The synthesis yield of stable material was evaluated thanks to the weight loss in the 600–700 °C range specific to carbon structures [56].

Carbon structure defects were assessed by Raman spectroscopy at 532 nm using a confocal Labram HR800UV (Horiba Jobin Ivon, Japan). The quality of the carbon structure surface layer was evaluated thanks to the I_D/I_G ratio calculated from averaged spectra obtained on three different locations of every sample. The Raman intensity of D-band (I_D) refers to the defects of the graphitic structures while the G-band intensity (I_G) corresponds to the orientation degree of the CNTs [50]. The D and G bands are observed in the 1300–1350 cm^{-1} and the 1570–1600 cm^{-1} ranges, respectively. The I_D/I_G ratio was calculated using pseudo- Voigt function, a combination Lorentzian and Gaussian deconvolution functions [57].

Scanning electron microscopy pictures (SEM) were obtained on a JSM-7900F (Jeol, Japan) coupled with an energy-dispersive X-ray spectroscopy analyzer (EDS). SEM images were used to calculate CNTs mean diameter and standard deviation using Image J software.

Note that TEM analysis (Transmission Electron Microscopy) might not be done as membrane thickness should not be reduced enough to achieve electron transparency.

2.3. Fractional factorial experimental design

As said above, the DoE methodology was applied throughout 5 parameters on 3 levels as shown in Table 1. For example, the synthesis temperature (denoted as parameter 1) was ranged from 650 to 850 °C, which is typical synthesis temperature reported in the literature [10,54].

As parameters were not expected to have a linear influence on responses in the chosen intervals, three different levels were defined in the investigated experimental design [53]. Consequently, in order to perform a regular design, 3^5 = 243 experiments would have been required. To reduce this number, it was decided to split the three levels into two adjacent 2^{5-2} fractional factorial designs (leading to a total of 16 experiments) where parameters main effects will be confounded with two factor interactions [58].

For example, the parameter Fe wt% in dip-coating solution (1) main effect denoted a_1, which quantify the influence of this parameter on the desired

response (i.e.: I_D/I_G ratio or C wt% yield), is aliased with a_{35}, corresponding to the effect of the interaction between the calcination temperature (parameter denoted (3)) and the CVD duration (denoted (5)).

These aliased effects are regrouped in the form of a contrast denoted $l_1 = a_1 + a_{35}$. Corresponding contrasts are detailed in Table 1 and were generated using I = 1234 = 135 generating relation. These parameters relationships allow to specifically study the interactions between C_2H_6 gas fraction (2) and both Fe in dip-coating solution (1) and calcination temperature (3), as suggested by Lu et al. [59]. More details about the methodology are given in the Supplementary data (see part A.1).

Table 1
Experimental designs levels values.

Parameters	Contrast aliasing (1st and 2nd order only)	Design 1 low level	Design 1 high level/design 2 low level	Design 2 high level
(1) Fe in dip-coating solution	$l_1 = a_1 + a_{35}$	0.5 wt%	1.5 wt%	2.5 wt%
(2) C_2H_6 gas fraction	$l_2 = a_2 + a_{45}$	10%	20%	30%
(3) Calcination temperature	$l_3 = a_3 + a_{15}$	200 °C	350 °C	500 °C
(4) CVD temperature	$l_4 = a_4 + a_{25}$	650 °C	750 °C	850 °C
(5) CVD duration	$l_5 = a_5 + a_{13} + a_{24}$	0.5 h	1 h	1.5 h

Significant contrasts were isolated using Lenth's procedure with a 90% confidence interval [60] (see Supplementary data part A.2 for details). Briefly, a Margin of Error (ME) value is calculated for each design. Contrasts having their effect over the ME value have a significant influence on the studied response in the design range. Then hypotheses (detailed in part A.1 of Supplementary data) are applied to identify relevant parameters regarding the I_D/I_G ratio and C wt% yield.

DoE generation and data treatment were performed thanks to R software [61] and the package FrF2 V1.7-2 [62]. Finally, the specific impact of C-CVD conditions on experimental results from DoE was investigated with R software using the deep learning package (Classification and Regression Training package (*caret*), version 6.0.80). Decision trees were obtained by linking C wt% and I_D/I_G ratio to CVD main parameters defined by DoE analysis and are based on ANOVA methodology with a complexity parameter (cp) equals to 0.05.

2.4. Membrane characterization

2.4.1. Pure water permeability (PWP)

In order to link membrane modification to filterability, specific synthesis conditions selected thanks to the DoE results were chosen and used to modify large membrane pieces (surface area of 55 cm^2). Prior to membrane permeability measurements, the membrane was sandwiched and glued (Araldite 2020 Huntsman Corporation, USA) between two Teflon pieces. Permeability was measured thanks to a labscale filtration pilot (Fig. S3 in Supplementary data). Filtration was carried out in submerged dead-end constant flux mode using a peristaltic pump (Masterflex L/S, Cole-Parmer, USA). Transmembrane pressure (TMP) was monitored every 10 s thanks to a − 1 to 1.6 bar UNIK 5000 sensor (GE, USA) and temperature was measured using a thermocouple (National Instruments, USA). Membrane permeability was evaluated throughout the constant flux step method consisting of 5 steps of 2 min each after flux was stabilized (Std Dev 2.3%). The permeability was calculated thanks to the Darcy law and normalized at 20 °C (see part A.3 in Supplementary data).

2.4.2. Underwater contact angle (UWCA)

The impact of SiC membrane functionalization on wettability was evaluated through underwater contact angle measurements (UWCA). Tests were conducted in the captive bubble mode since the investigated membrane was too porous to sustain droplets at its surface in air. Therefore, oil droplets (6 µL) sampled from Total Activa 5000 15W-40 engine oil (density at 15 °C of 0.888 $kg \cdot m^{-3}$, API gravity of 28° and a dynamic viscosity at 40 °C of 110 $mm^2 \cdot s^{-1}$) were released at the membrane surface being submerged under a 88 $mg \cdot L^{-1}$ sodium dodecyl sulfate (SDS) anionic surfactant solution (Sigma Aldrich) diluted in MilliQ water. Engine oil surface tension was measured as 24 $mN \cdot m^{-2}$. Fig. S4 shows the measurement principle and experimental setup, respectively. UWCA was measured using a drop shape analyzer DSA25 (Kruss, Germany) and measurements were done in triplicate on every investigated sample (Std Dev 5.8%).

2.4.3. Conductivity measurements

Crushed and sieved at 50 µm membrane samples were placed in Solartron (Solartron Metrology, Germany) 12962A Sample Holder. Electrochemical impedance spectra (EIS) were acquired at open circuit voltage with a Solartron SI1287 electrochemical interface and an SI1260 impedance/gain-phase analyzer with an amplitude of 10 mV in the 10 Hz to 10 kHz frequency range. Each measurement was done in triplicate and gave access to the electrical impedance by measuring electrical resistance R and the phase difference, between voltage and current, called phase angle θ. Conductivity was calculated by modeling every sample as a resistance and a capacitor in parallel or in series and were deducted from the measurement of the complex impedance.

The phase angle (θ), calculated from the Bode diagram at 1 kHz, gives information about the general behavior of the material at this frequency. For example, a material acting as a capacitor will return a phase angle closed to −90° while a pure electrical resistance will exhibit a phase angle close to 0°.

2.4.4. Dielectric permittivity

SiC/CNTs composite membranes have great potential as microwave absorbing materials [63]. For this purpose, the two parts of the relative complex permittivity ε_r' and ε_r'' were evaluated. Crushed and sieved at 50 µm membrane samples were analyzed as described in previous work [64]. The complex permittivity of the composite materials was measured in triplicate in the range of 2–18 GHz at 26 °C thanks to an Agilent PNA_L series N5230A vector network analyzer (Agilent Technologies, USA). Briefly, ε_r' and ε_r'' are the real and the imaginary parts of the relative complex permittivity of a material. The storage of electromagnetic energy is expressed by the real part while the thermal conversion is proportional to the imaginary part [65].

3. Results and discussion

3.1. Main CVD influencing parameters

Results for TGA and Raman responses from the two experimental designs are reported in Table 1 and calculated contrast values are presented in Table 2. Calculation method is detailed in Supplementary data (Section A.1). First of all, the TGA response (corresponding to carbonaceous materials yield) throughout the experimental designs will be discussed followed by the Raman response (corresponding to carbonaceous material structure).

Table 2

3.1.1. TGA response

TGA response is here helpful to quantify the amount of stable carbon material grafted on the membrane. It is important to note that only strongly attached carbonaceous materials were considered due to the intensive ultrasonic cleaning performed. As it can be seen throughout all experimental conditions investigated and reported in Table 2, the highest amount of attached carbonaceous materials synthesized on the membrane was equal to 4.71% obtained on the run #16. In contrast the lowest amount was obtained for the run #5 and was equal to 1.01%.

Also, 1.42% of carbon materials were synthesized with almost all the lowest parameter levels during run #1. Weight loss equals to 2.78% was

obtained with the mid-ranged levels during run #8 which is closed to the average TGA results (mean value equals to 2.48% over the two designs).

This increasing trend shows that CVD input parameters have an overall positive effect on the amount of carbon grafted on the membrane and match with expectations: the more the catalyst deposited on the substrate (influenced by parameter (1)) the more nucleation sites for carbon synthesis which will be kinetically promoted by parameters 2 (gas ratio), 4 (temperature) and 5 (CVD duration). Parameter by parameter interpretation of the results reported in Table 2 would not be convenient as experimental runs are independent. This analysis can be done quickly by looking at Fig. 2 where significant parameters according to Lenth method with a 90% confidence interval are highlighted.

For TGA response, Fe wt% in dip-coating solution (1), CVD duration (4) and temperature (5) are the most significant parameters in the studied experimental range. These results can be supported by analyzing the contrast values of Table 3. It is important to note that calculated values correspond to contrasts, which are aliases of parameter effects and two parameters interactions.

For the design 1 range, I_2, I_4, I_{12} and I_{23} are negligible (values close to 0). Consequently, α_2, α_{24}, α_4, α_{15}, α_{12}, α_{34}, α_{23}, α_{14} and α_{24} can be neglected. This means that C_2H_6 gas fraction (2) and CVD temperature (4), as well as the cited two parameters interactions, did not impact the quantity of attached carbonaceous material on the membrane in this range. On the other hand, $I_1 = \alpha_1 + \alpha_{35}$ and $I_5 = \alpha_5 + \alpha_{13} + \alpha_{24} \simeq \alpha_5 + \alpha_{13}$ contrasts were significant. $I_3 = \alpha_3 + \alpha_{15}$ is neither significant nor negligible, so a α_{35} and α_{13} cannot be neglected. However, I_3 value could be a consequence of α_{15}, as the interaction of two significants contrasts can be significant.

Calcination temperature (3) is expected to have an influence on catalyst morphology. This influence might be emphasized by comparing run #3 and run #7 by SEM on Fig. 3. These two samples only differ by their CVD duration (5) (0.5 h for #7 and 1 h for #3) and calcination temperature (3) (200 °C for #3 and 350 °C for #7). As shown on Fig. 3 the iron catalyst exhibited a nanorod-like particles shape at lower calcination temperature whereas at higher calcination temperature

: 2^{5-2} experimental designs levels with $I = 1234 = 135$ generator with TGA and Raman responses.

Run	(1) Fe in dip-coating solution	(2) C_2H_6 gas fraction	(3) Calcination temperature	(4) CVD temperature	(5) CVD duration	TGA results (C weight %)	Raman results (I_D/I_G)
1	0.5%	10%	200 °C	650 °C	1 h	1.42	0.93
2	1.5%	10%	200 °C	750 °C	0.5 h	1.55	0.91
3	0.5%	20%	200 °C	750 °C	1 h	1.73	1.01
4	1.5%	20%	200 °C	650 °C	0.5 h	1.44	1.11
5	0.5%	10%	350 °C	750 °C	0.5 h	1.01	1.11
6	1.5%	10%	350 °C	650 °C	1 h	2.40	0.93
7	0.5%	20%	350 °C	650 °C	0.5 h	1.33	0.94
8	1.5%	20%	350 °C	750 °C	1 h	2.78	0.97
9	1.5%	20%	350 °C	750 °C	1.5 h	2.87	1.08
10	2.5%	20%	350 °C	850 °C	1 h	3.21	1.48
11	1.5%	30%	350 °C	850 °C	1.5 h	4.17	1.66
12	2.5%	30%	350 °C	750 °C	1 h	2.86	1.13
13	1.5%	20%	500 °C	850 °C	1 h	2.94	1.37
14	2.5%	20%	500 °C	750 °C	1.5 h	2.89	1.08
15	1.5%	30%	500 °C	750 °C	1 h	2.43	1.05
16	2.5%	30%	500 °C	850 °C	1.5 h	4.71	1.56

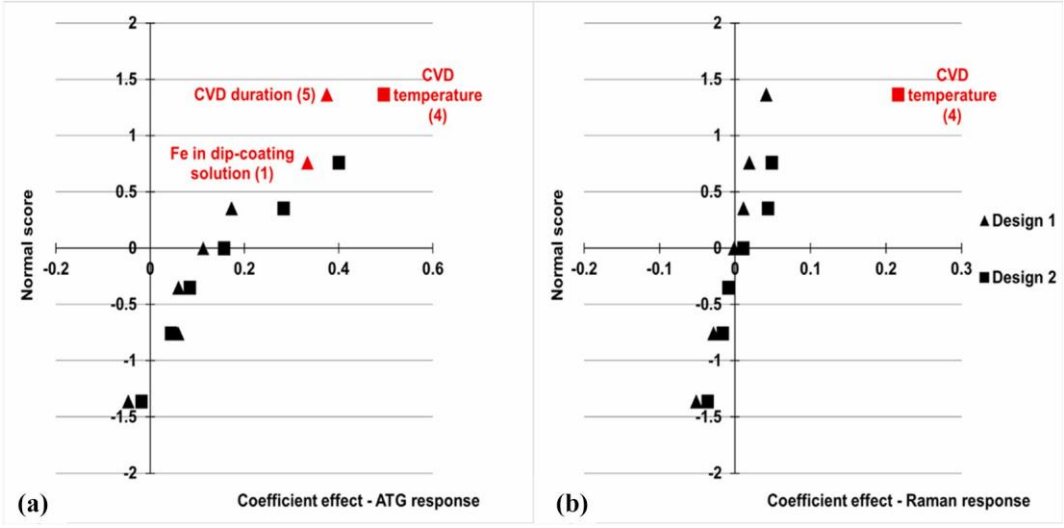

Fig. 2. Daniel plot on a) TGA response and b) Raman response. Named parameters are significant according to Lenth method with a 90% confidence interval.

Table 3
Contrast effects of growth factors on TGA and Raman responses in codded value.
Significant values (above Margin of Error) are bold and underlined.

Parameters	Contrast	TGA response		Raman response	
		Effect in design 1 range	Effect in design 2 range	Effect in design 1 range	Effect in design 2 range
ME with 90% confidence interval		±0.22	±0.45	±0.07	±0.10
(1) Fe in dip-coating solution	$I_1 = \alpha_1 + \alpha_{35}$	**0.33**	0.16	− 0.01	0.01
(2) C_2H_6 gas fraction	$I_2 = \alpha_2 + \alpha_{45}$	0.11	0.28	0.02	0.05
(3) Calcination temperature	$I_3 = \alpha_3 + \alpha_{15}$	0.17	− 0.02	0.00	− 0.04
(4) CVD temperature	$I_4 = \alpha_4 + \alpha_{25}$	0.06	**0.50**	0.01	**0.22**
(5) CVD duration	$I_5 = \alpha_5 + \alpha_{13} + \alpha_{24}$	**0.38**	0.40	− 0.03	0.04
(1)-(2) interaction	$I_{12} = \alpha_{12} + \alpha_{34}$	− 0.05	0.08	0.04	− 0.02
(2)-(3) interaction	$I_{23} = \alpha_{23} + \alpha_{14}$	0.06	0.04	− 0.05	− 0.01

more spherical particles were observed. It is highly unlikely that CVD duration (5) impact the catalyst morphology, so the difference between the rod like and the seed like catalyst structure was due to the calcination temperature (3) difference (run #3 and #7, respectively).

The "seed like" geometry is required as the catalyst acts as a base for the growth of the nanotubes. In contrast a rod like catalyst particle would less likely give rise to a CNTs as it may be inactive FeOOH [66] and be not suitable for CNTs growth. Consequently, calcination temperature (3) cannot be neglected but can be classified as less impactful compared to Fe wt% in dip-coating solution (1) and CVD duration (5) parameters in the design 1 range.

For the design 2 range, I_3, I_{12} and I_{23} are negligible. Consequently, α_3, α_{15}, α_{35}, α_{13}, α_{34}, α_{23}.and α_{14} can be neglected. Calcination temperature (3) is not influent on the response in this range (350 °C–500 °C). CVD temperature (4) was the only coefficient identified as significant by Lenth method, but CVD duration (5) and C_2H_6 gas fraction (2) were not negligible. However, their value could be a consequence of their aliasing, $I_5 = \alpha_5 + \alpha_{24}$ and $I_2 = \alpha_2 + \alpha_{45}$. The interaction coefficients may contribute to the contrast values as α_{24} and α_{45} are interactions between the significant parameter and not negligible parameters. According to

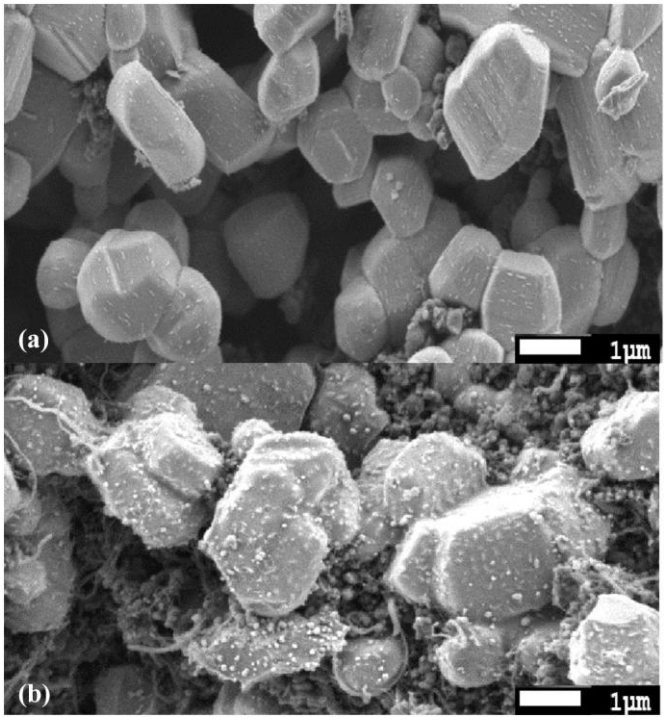

Fig. 3. Fe_2O_3 structure for samples of experiments a) #2 with calcination temperature of 200 °C and b) #7 with calcination temperature of 350 °C.

results presented in Table 3, the effect of the Fe wt% in dip-coating solution (1) is small compared to the effects of (2), (4) or (5) parameters but not negligible.

Results corresponding to the design 2 indicate that the CVD temperature has a strong impact on the C wt% yield of anchored carbon structure at the membrane surface.

To conclude, these two DoE confirmed that the Fe wt% in dip-coating solution (1) influenced the carbon yield, as the more catalyst deposited on the membrane the more nucleation sites for carbon growth are available. More precisely parameter 1 (Fe wt% in dip-coating solution) was found significant according to Lenth method in the design 1 range (Table 3) and having a non-negligible influence in the design 2 range.

In contrast, C_2H_6 gas fraction (2) showed in both designs a limited influence on the carbonaceous materials yield compared to the other studied parameters within the investigated experimental range.

Results suggest that calcination temperature (3) presents a threshold value between 200 and 350 °C where catalyst morphology and structure inhibits carbon growth, due to a change in catalyst structure and composition [66].

CVD temperature (4) showed the strongest effect in the highest range of temperature, while being not influent in the low range of considered temperature. CVD temperature is expected to impact the kinetic of carbon growth, but also the structure of the CNTs [53]. As shown here, increasing the CVD temperature from 750 °C to 850 °C might induce a structure change in the carbon layer making it more suitable for attachment leading consequently to less synthesized carbon particles removed during ultrasonic cleaning. It was indeed observed visually that less carbon was removed by the ultrasonic treatment for samples synthesized at high temperatures. Finally, regarding the synthesis yield, the CVD duration (5) was found significant according to Lenth method in the low range of investigated values. As expected, the longest the CVD duration, the more carbon is synthesized as more carbon is fed to the catalyst for the growth of the CNTs until it becomes inactive.

3.1.2. Raman response

Raman response is used here to analyze the defects in the synthesized carbonaceous structure and consequently to differentiate the different carbon allotropes. Usually the G-band is associated with an ideal sp^2 graphitic lattice while the D-band corresponds to defects, such as amorphous carbon, curvature in the graphitic lattice or disordered lattices [67]. Looking at Table 3 and the Raman response, calculated I_D/I_G ratio was ranged from 0.91 to 1.66, for samples #2 and #11 respectively. Raman response can be classified in three clusters depending on their values: (cluster I) samples #1, #2, #3, #6, #7 and #8 response values were between 0.91 and 1.01; (cluster II) samples #4, #5, #9, #12, #14 and #15 between 1.05 and 1.13 and (cluster III) samples #10, #11, #13 and #16 between 1.48 and 1.66.

It is commonly reported that the higher the CVD temperature (5) the higher the I_D/I_G ratio value is [68]. The temperature dependence of the I_D/I_G ratio suggests a lower activation energy at high temperature leading to the formation of more defects.

According to the Lenth method analysis of Table 3, the unique significant parameter over the two designs is the CVD temperature (4).

In the design 1 range, response variations of I_D/I_G ratio were not important enough to quantify the effect of investigated parameters. Indeed, all the contrasts reported on Table 3 can be neglected.

In the design 2, the only significant contrast effect is the synthesis temperature ($I_4 = a_4 + a_{25} \approx a_4$). Note that all other contrasts and corresponding interactions were negligible, so the interactions effect between the gas ratio and CVD duration (a_{25}) can be neglected. As shown in Table 2, increasing the CVD temperature from 750 to 850 °C led to higher I_D/I_G ratios, characteristic of a more disordered carbonaceous structure. This difference can be observed on Fig. 4. When I_D/I_G is equals to 0.94, D and G peaks were sharp and the observed CNTs average diameter was equal to 40.5 ± 3.4 nm. In contrast, for I_D/I_G equals to 1.48, Raman peaks are broad, especially the D band and CNTs average diameter was higher and equals to 84.7 ± 8.3 nm. A higher I_D/I_G ratio is

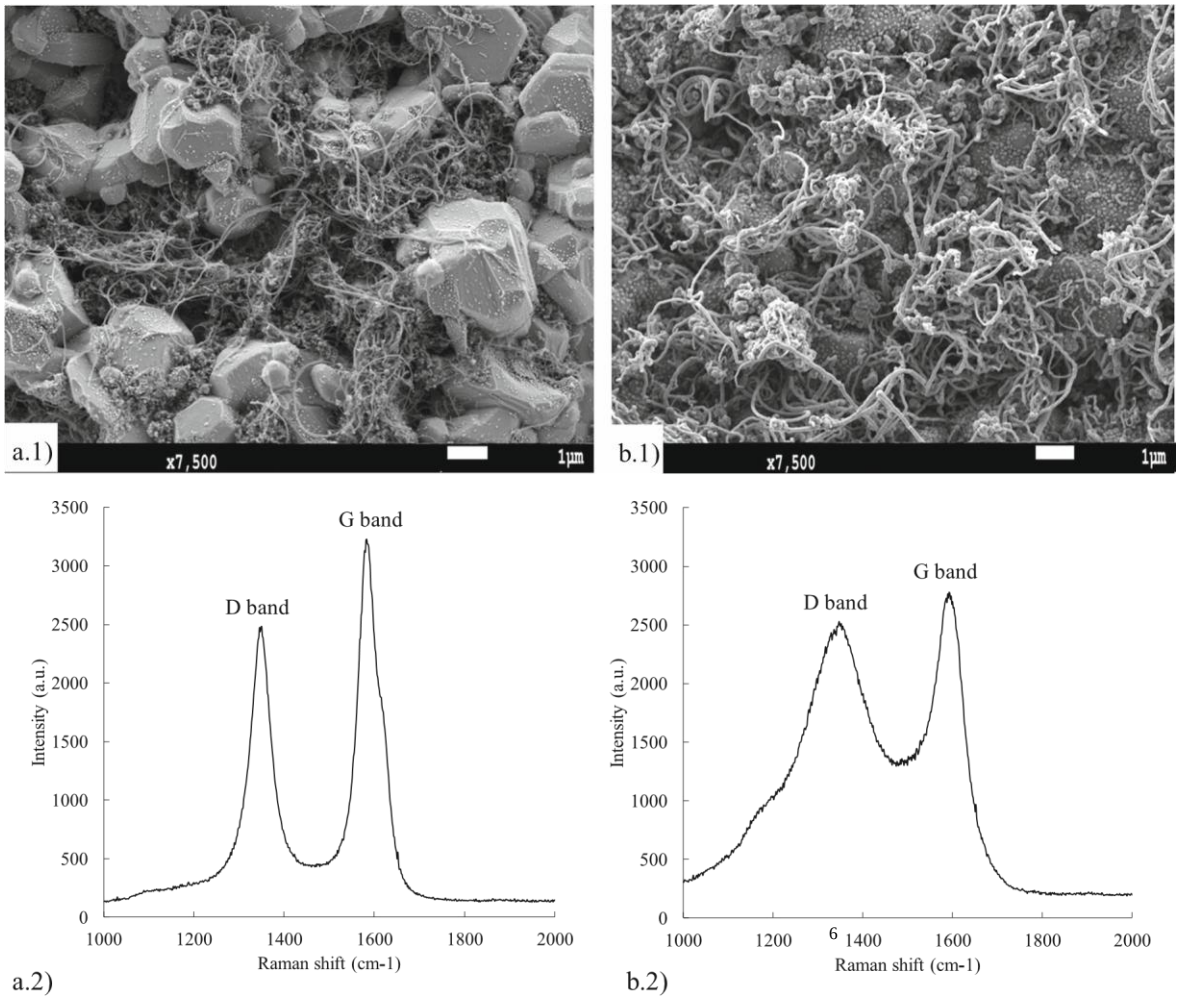

Fig. 4. SEM picture and associated Raman spectra of samples a) #7, I_D/I_G = 0.94 and b) #10, I_D/I_G = 1.48.

consequently related to larger CNTs, were synthesized at higher temperature. This fit with theory as CNTs with a bigger diameter show more defects and higher I_D/I_G ratio [49].

3.1.3. DoE conclusion

The DoE used in this study revealed that the carbonaceous materials structure synthesized on SiC membrane showed a drastic change for CVD temperature above 750 °C. Indeed, it was found that increasing CVD temperature led to larger CNTs and less structured carbon particles (higher I_D/I_G ratio). CVD temperature (4) showed influence for both TGA and Raman responses for temperature above 750 °C while no influence was observed for lower temperature. According to the intensive cleaning performed on functionalized samples, this result suggests that CNTs with more defects and bigger diameter are more prone to better attachment at the SiC membrane surface.

Regarding the synthesis yield, the three most influencing parameters were found to be the Fe wt% in dip-coating solution (1), CVD temperature (4) and CVD duration (5) whatever the considered range. It was also observed that the catalyst calcination temperature showed a threshold value between 200 and 350 °C which might be linked to the catalyst properties (nature and morphology).

Finally, based on DoE conclusion, regression trees were built by linking I_D/I_G ratio and synthesis yield to the main CVD parameters (Fig. 5-a and b, respectively). As shown on Fig. 5, the most influencing parameters is the CVD temperature in both trees (first node). Concerning the I_D/I_G ratio results, the regression tree methodology reported 5 clusters with a strong change for temperature above 800 °C (Fig. 5-a). All samples, synthesized at 750 °C, are regrouped in the same cluster (cluster A: sample # 2; 3; 5; 8; 9; 12; 14; 15) due to their similar I_D/I_G ratio. Also, it can be seen a slight influence of CVD duration for sample synthesized at 650 °C and 850 °C (Cluster B, C and D, E respectively). Interestingly, the corresponding Raman spectra showed that the 2D band drastically decreased with the increasing temperature. As previously reported, the decreasing intensity of the 2D band might be related to the thickness of the carbon nanotubes [69].

Concerning the synthesis yield, the regression tree reported 5 clusters (Fig. 5-b). The same clusters, as for regression tree based on Raman analysis (Fig. 5-a), were found for high temperature (cluster D and E for temperature above 850 °C) indicating that the CVD duration is an important parameter at high temperature. For lower synthesis temperature and for long CVD duration, it appears that the Fe wt% in dip- coating solution parameter influence the synthesis yield. This is confirmed by the SEM pictures corresponding to every cluster reported on Fig. 5-b. As shown a large amount of CNTs with large diameter were synthesis at high temperature. For lower temperature, the porous SiC membrane might be observed and CNT exhibited small diameter as previously discussed.

In terms of membrane filtration functionalization, it might be assumed that a large quantity of CNTs exhibiting more defects would be preferable. Indeed, more defects would increase hydrophilicity [70] and would provide several sites for further CNTs modifications (i.e.: grafting of TiO_2, MnO_2, dopamine…). Consequently, our results suggest that SiC/CNTs composite membranes should be fabricated according to parameters in the design 2 range and at a CVD temperature of 850 °C for a duration of at least 1 h (corresponding to Cluster D or E, Fig. 5).

In order to investigate the impact of CNTs synthesis conditions on membrane performances, specific CVD conditions listed in Table 4 were chosen for the scale-up. These conditions correspond to the cluster D and A in Fig. 5 for membranes 1; 2; 4 and membrane 3, respectively.

3.2. Impact on physical properties

The DoE methodology emphasized the strong influence of three parameters on the quantity and the structure of the synthesized carbon layer: Fe wt% in dip-coating solution (1), CVD temperature (4) and CVD duration (5). These three parameters are more precisely studied towards their impact on the membrane surface wettability through pure water permeability and UWCA, as well as electronic properties. Four membranes were synthesized at a larger scale (55 cm^2) by changing one of the previously mentioned parameters at a time and keeping the C_2H_6 gas fraction (2) at 20% and calcination temperature (3) at 350 °C constant. Synthesis conditions and corresponding properties are summarized in Table 4. One can notice that whatever the investigated CVD conditions, the scale up process led to lower C weight % yield which might be due to the smaller specific surface of the large membranes due to their larger thickness, for a constant gas fraction and a potential change in CVD reactor hydrodynamics. *3.2.1. Membrane surface wettability*

3.2.1.1. Pure water permeability (PWP). The highest PWP equals to 15,685 $L\cdot m^{-2}.h^{-1}.bar^{-1}$ was obtained for the pristine SiC membrane indicating that the CNTs synthesis process induced an increase of the membranes' hydraulic resistance. According to reported results, the PWP decreased with the increasing synthesized C weight % on the membrane (Fig. 6-a). More specifically a minimum of 1308 $L\cdot m^{-2}.h^{-1}.bar^{-1}$ was achieved for Mem#1, with the highest levels of all synthesis parameters. Decreasing the Fe wt% in dip-coating solution (1) from 1.5% to 0.5% increased the permeability by a factor 2 compared to Mem#1 (from 1308 to 2652 $L\cdot m^{-2}.h^{-1}.bar^{-1}$, respectively). Reducing the CVD temperature (4) from 850 to 650 °C increased the PWP more drastically from 1308 to 8513 $L\cdot m^{-2}.h^{-1}.bar^{-1}$ for Mem#1 and Mem#3, respectively.

According to previous DoE analysis, Fe wt% in dip-coating solution (1) and CVD duration (5) were determined to only influence the carbon quantity at the membrane surface. This was confirmed visually by SEM analysis (Fig. 6-c) where a mix of amorphous carbon and CNTs can be observed on samples Mem#1 and Mem#2 (SEM analysis of Mem#4 was similar to Mem#2 and Mem#1).

In contrast and as demonstrated by the DoE in Section 3.1, changing the CVD temperature (5) might impact both quantity and structure of the carbon surface layer. This was confirmed by a more drastic decrease of C weight % for Mem#3 compared to Mem#1 from 0.88 to 1.55%, respectively. In addition, no CNTs and only amorphous carbon might be identified at the Mem#3 surface from the SEM analysis (Fig. 6-c.1).

These results demonstrate that carbon layer synthesized at the SiC membrane surface blocks membrane pores and consequently decreases membrane PWP. Similar results were observed by Yuan et al. (2020) regarding a drastic loss of gas permeability of SiC support after the growth of CNTs [32].

3.2.1.2. Underwater contact angle (UWCA). In addition to membrane's pore blockage due to carbon layer synthesis, the decrease in PWP might be due to a change in hydrophilicity. The hydrophobic effect of the synthesized carbon layer was assessed by UWCA measurements and results are summarized on Table 4 and Fig. 6-b.

As expected, the pristine SiC was the most hydrophilic materials with a UWCA equals to 138.8 ± 6.2°, while the lowest UWCA were obtained for both Mem#1 and Mem#2 samples. Obviously, the CNTs synthesis at the membrane surface strongly reduced the SiC membrane hydrophilic property.

As depicted on Fig. 6-b, the PWP is well correlated to UWCA. The hydrophobicity of CNTs can be more precisely observed by comparing Mem#3 and Mem#4. Mem#3 can be considered as hydrophilic with an UWCA > 90° while Mem#4 is hydrophobic with an UWCA < 90°. These two samples have similar carbon content (C wt% equal to 0.88 and 1.01%, respectively) but different carbon layer structures. Specifically, amorphous carbon was synthesized at a low temperature of 650 °C on Mem#3 while Mem#4 carbon layer consisted mainly of CNTs synthesized at a higher temperature of 850 °C. Consequently, the strong PWP difference between Mem#3 and Mem#4 might be explained by the

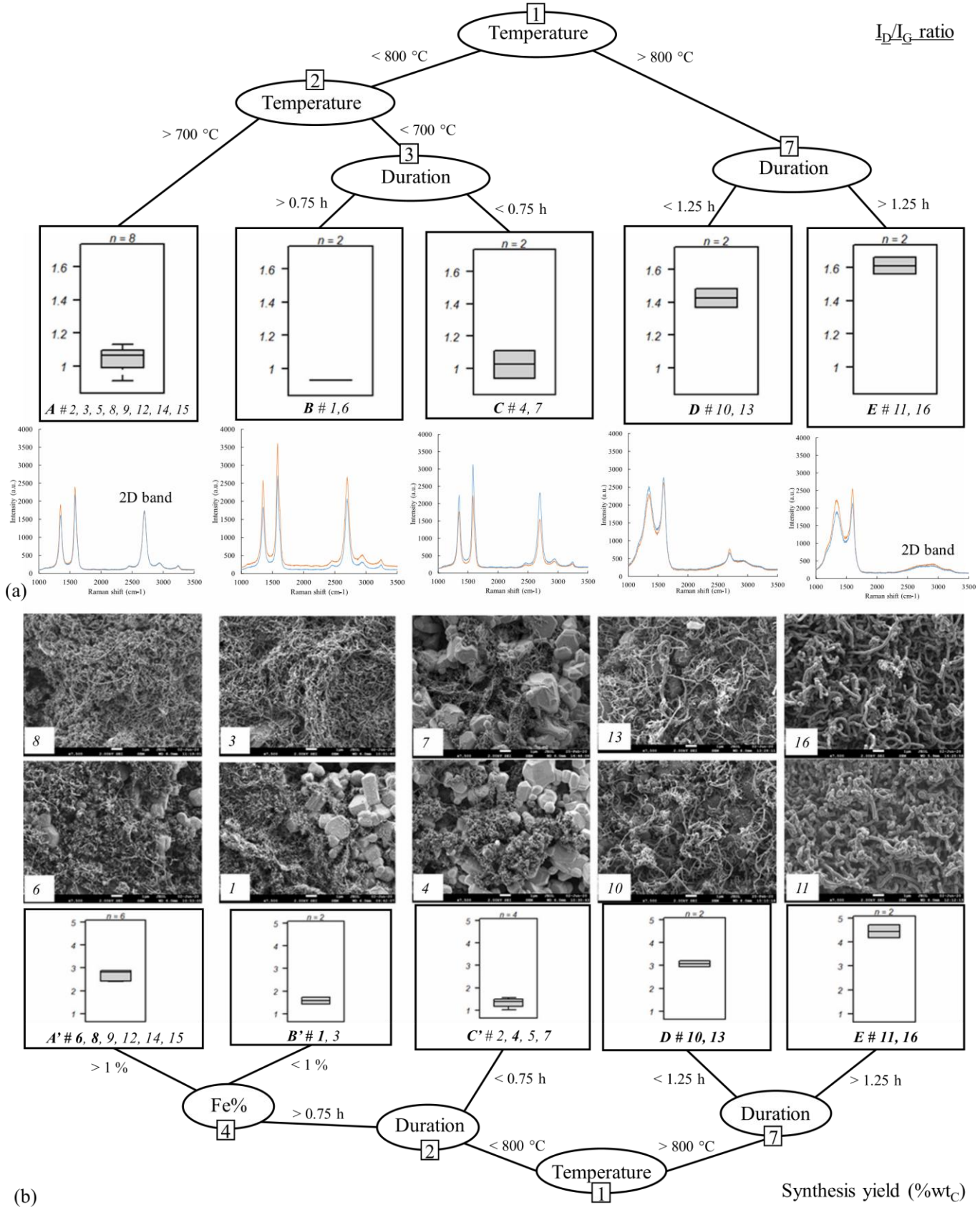

Fig. 5. Regression trees performed on the DoE results based on I_D/I_G ratio (a) and synthesis yield (%wt_C) (b). SEM pictures give information on the structure of the corresponding CNT layer. "#" Symbol denotes the sample number in corresponding cluster. SEM scale is 1 µm and 7500 magnificence on all images.

Table 4
Summary of the wettability and electronic properties of the pristine and composite SiC membrane synthesized for water filtration. Calcination temperature was fixed to 350 °C and C_2H_6 gas fraction to 20%.

	Pristine SiC	Mem#1	Mem#2	Mem#3	Mem#4
(1) Fe in dip-coating solution	/	1.5%	0.5%	1.5%	1.5%
(4) CVD temperature	/	850 °C	850 °C	650 °C	850 °C
(5) CVD duration	/	1 h	1 h	1 h	0.5 h
C weight % (TGA response)	0% 15,685	1.55% 1308	1.37% 2652	0.88% 8513	1.01% 3589
Lp (L· m⁻²· h⁻¹· bar⁻¹)					
UWCA (°)	138.8 ± 6.2	55.3 ± 12.9	57.0 ± 10.9	100 ± 17.0	65.4 ± 15.4
Phase angle (°)	− 90	− 1	0	− 76	− 15
Calculated conductivity ($S.m^{-1}$)	$(11.40 \pm 5.79) \times 10^{-4}$	$(5.46 \pm 1.48) \times 10^{-1}$	$(23.40 \pm 2.47) \times 10^{-3}$	$(26.00 \pm 7.56) \times 10^{-4}$	$(15.80 \pm 5.03) \times 10^{-4}$

Fig. 6. Impact of the 3 chosen synthesis parameters on a) water permeability Lp, b) underwater contact angle and c) Surface morphology of the membrane observed

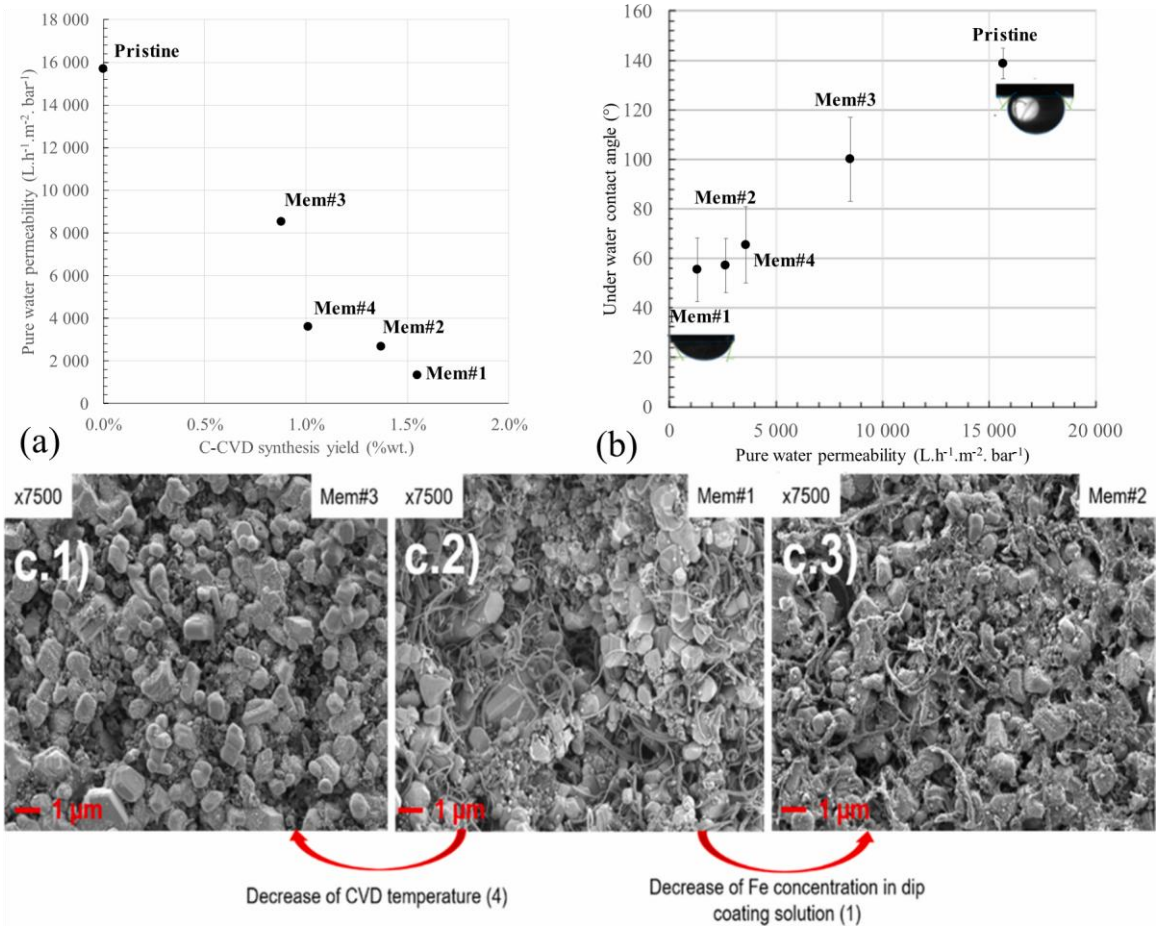

by SEM. drastic decrease of UWCA due to anchored CNTs induced by a higher CVD synthesis temperature.

3.2.2. Surface electronic properties

3.2.2.1. Conductivity. The development of one step process coupling membrane separation and electrochemical oxidation is considered as a breakthrough innovation to separate and degrade simultaneously pollutants [71–73].

The presence of CNTs on the SiC membrane might offer a conductive network which could promote electron transfer. Consequently, the electrical properties of the developed SiC/CNTs composite membranes were evaluated through EIS. The phase angle and conductivity, obtained from the Nyquist and Bode Plots (Fig. S5 of Supplementary data), were reported on Table 4 and Fig. 7. It is important to note that the low electrical conductivity values and high standard deviation obtained are related to the measurement method which was done on porous bed made with 50 µm crushed membranes samples (estimated porosity ~ 0.35%).

As shown in Table 4, the pristine SiC membrane might be considered as a pure capacitor with a phase angle of − 90° and low electrical conductivity of $(11.40 \pm 5.79) \times 10^{-4}$ S· m^{-1}.

The carbon layer coating strongly influenced the phase angle θ. Indeed, as C wt% increased the phase angle was getting close to 0° (Fig. 7) and the electrical conductivity increased, indicating that the modified membranes might be modeled as electrical resistances.

There is a drastic change between Pristine SiC, Mem#3 and Mem#1, #2 and #4 where membrane's electrical properties switches from capacitor to electrical resistance. This modification was attributed to the presence of CNTs obtained at higher CVD temperature (i.e.: 850 °C for Mem#1, #2 and #4).

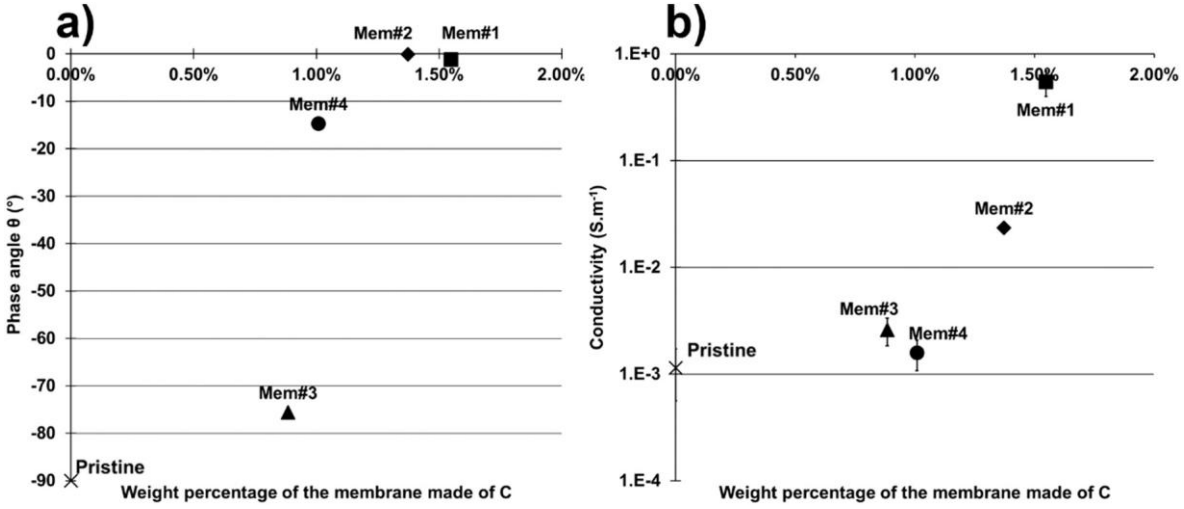

Fig. 7. a) Phase angle and b) membrane conductivity as a function of C weight percentage.

According to the electrical conductivity values, there is a threshold value around 1.4% C wt above which the CNTs network starts to better transfer electrons (Fig. 7). Lanfant et al. (2019) observed a similar behavior with a drastic decrease of electrical resistivity with increasing CNTs amount in SiC/CNTs composite materials [74]. As shown by the Nyquist Plots (Fig. S5 in Supplementary data), the pristine membrane might be modeled as an electrical resistance and a capacitor in series. The Nyquist plot of Mem#3 showed a typical electronic transfer phenomenon linked to a potential oxidation of the iron catalyst.

To conclude, presented results demonstrate that the SiC/CNTs composite membrane could transfer electron and that the electrical conductivity depends on the CVD synthesis conditions. Changing the CVD temperature (4) will impact the electrical nature of the synthesized materials and increasing the synthesis C wt% yield by changing the Fe wt% in dip-coating solution (1) and/or CVD duration (5) will impact the electrical conductivity of the materials.

3.2.2.2. Permittivity. A recent study by Fu and Zhang [75] demonstrated the effect of MW on porous membranes regarding pollutant degradation and membrane fouling prevention due to local heating and to the formation of nanobubbles on hydrophobic membrane surface. Consequently, permittivity measurements were conducted on Mem#1 to assess if the coating with the highest amount of CNTs was efficient to fulfill the previously exposed objectives for water treatment.

As shown on Fig. S6 in Supplementary data, the investigated membranes exhibited a classical dielectric dispersion versus the frequency. In this frequency range, the dipolar polarization is the most significant phenomena [76].

For the pristine SiC membrane, the real part of the permittivity (ε_r') was slightly decreasing from 12 to 11 between 1 and 20 GHz. The imaginary part of the permittivity (ε_r'') was slightly increasing from 0 to 2 in the same frequency range. More precisely ε_r' and ε_r'' were equal to 12.0 ± 1.0 and 0.28± 0.02 at a specific frequency of 2.45 GHz (Table 5). In contrast, the permittivities of the Mem#1 material were both decreasing from around 90 to 18 within the same frequency range. At 2.45 GHz, the ε_r' was around 4 times higher for the CNTs membrane than

Table 5
Relative dielectric permittivity at 2.45 GHz and 26 °C.

Sample	Real part ε_r'	Imaginary part ε_r''
Pristine SiC	12.0 ± 1.0	0.28 ± 0.02
Mem#1	47.10 ± 0.09	39.8 ± 2.4

for the pristine and was equal to 47.1 ± 0.09, and ε_r'' was more than 100 times higher. These results confirmed that the composite membrane material is more susceptible to absorb microwave radiations, then dissipate them as heat. Consequently, the SiC/CNTs composite material will be more energetically efficient than a pristine membrane towards interaction with microwaves which might be beneficial for a use in water treatment [77].

4. Conclusion

The objectives of the present work were to investigate the impact of CVD parameters on the properties of small SiC/CNTs nanocomposite membranes (3 cm^2). To this end, a fractional factorial experimental design was used in order to quantify the influence of interaction effects between the CVD process parameters. Regarding the synthesis yield, the three most influencing parameters were found to be the Fe wt% in dip- coating solution, CVD temperature and CVD duration. It was also observed that the catalyst calcination temperature showed a threshold value between 200 and 350 °C which might be linked to the catalyst properties (switching from rod to seed like particles). The DoE clearly revealed that higher CVD synthesis temperature (above 750 °C) led to larger CNTs and less structured carbon particles (higher I_D/I_G ratio). Synthesized CNTs were more prone to better attachment at the SiC membrane surface with a maximum synthesis yield equals to 4.71 C wt% despite intensive ultrasonic purification. In addition, it was demonstrated that the CVD process might be controlled to modify larger membrane surface area (55 cm^2) with desired properties. First, it was observed that the pure water permeability of the modified membranes was anti-correlated to the C wt% yield. The SiC/CNTs membranes exhibited much lower values than the pristine SiC microfiltration due to an increase of hydrophobicity with C wt% and potential pore blockage induced by the CNTs growth. Moreover, the electrical behavior switched from pure capacitor for the pristine membrane to pure electrical resistance with the increasing CVD temperature. Similarly, the SiC/CNTs membrane synthesized with the highest CVD parameters levels exhibited good microwave absorption properties related to a strong increase of its permittivity. To conclude, this study demonstrates that the hydraulic and electronic properties of SiC/CNTs nanocomposite membranes might be easily controlled through CVD synthesis conditions. The developed membrane material is currently used to investigate its antifouling properties regarding separation of industrial effluents.

Declaration of competing interest

The authors declare that they have no known competing financial interests or personal relationships that could have appeared to influence the work reported in this paper.

Acknowledgements

The authors acknowledge financial support from the European Union (ERDF) and “Region Nouvelle Aquitaine”. The authors would like to thank Michel Chauveau and Claud Veit from IC2MP for engineering the filtration and CVD setup respectively. Nadia Guignard from IC2MP- PLATINA for providing Raman expertise, Julie Rousseau from IC2MP- PLATINA for providing SEM expertise and Cl´ement Comminges from IC2MP for the access and counsel on EIS analysis, as well as Isabelle Polaert of LSPC in INSA Rouen for permittivity measurements.

Appendix A. Supplementary data

Supplementary data to this article can be found online at https://doi.org/10.1016/j.diamond.2021.108611.

References

[1] K.L. Jepsen, M.V. Bram, S. Pedersen, Z. Yang, Membrane fouling for produced water treatment: a review study from a process control perspective, Water 10 (2018) 847, https://doi.org/10.3390/w10070847.

[2] H. Nagasawa, T. Omura, T. Asai, M. Kanezashi, T. Tsuru, Filtration of surfactant-stabilized oil-in-water emulsions with porous ceramic membranes: effects of membrane pore size and surface charge on fouling behavior, J. Membr. Sci. 610 (2020), 118210, https://doi.org/10.1016/j.memsci.2020.118210.

[3] R.W. Field, D. Wu, J.A. Howell, B.B. Gupta, Critical flux concept for microfiltration fouling, J. Membr. Sci. 100 (1995) 259–272, https://doi.org/10.1016/0376-7388(94)00265-Z.

[4] S. Huang, R.H.A. Ras, X. Tian, Antifouling membranes for oily wastewater treatment: interplay between wetting and membrane fouling, Curr. Opin. Colloid Interface Sci. 36 (2018) 90–109, https://doi.org/10.1016/j.cocis.2018.02.002.

[5] Y.O. Raji, M.H.D. Othman, N.A.H.S.M. Nordin, M.R. Adam, Z.S. Tai, J. Usman, A. F. Ismail, Surface matrix functionalization of ceramic-based membrane for oil- water separation: a mini-review, Korean J. Chem. Eng. 37 (2020) 1631–1641, https://doi.org/10.1007/s11814-020-0575-5.

[6] H.Y. Lee, Y.H. Park, K.H. Ko, Correlation between surface morphology and Hydrophilic/Hydrophobic conversion of MOCVD– TiO2 films, Langmuir 16 (2000) 7289–7293, https://doi.org/10.1021/la9915567.

[7] D. Lu, T. Zhang, L. Gutierrez, J. Ma, J.-P. Crou´e, Influence of surface properties of filtration-layer metal oxide on ceramic membrane fouling during ultrafiltration of oil/water emulsion, Environ. Sci. Technol. 50 (2016) 4668–4674, https://doi.org/10.1021/acs.est.5b04151.

[8] Y.-P. An, J. Yang, H.-C. Yang, M.-B. Wu, Z.-K. Xu, Janus membranes with charged carbon nanotube coatings for deemulsification and separation of oil-in-water emulsions, ACS Appl. Mater. Interfaces (2018), https://doi.org/10.1021/ acsami.7b19700.

[9] H. Li, L. Daukiya, S. Haldar, A. Lindblad, B. Sanyal, O. Eriksson, D. Aubel, S. Hajjar-Garreau, L. Simon, K. Leifer, Site-selective local fluorination of graphene induced by focused ion beam irradiation, Sci. Rep. 6 (2016) 19719, https://doi.org/10.1038/srep19719.

[10] D.T. Tran, G. Thieffry, M. Jacob, C. Batiot-Dupeyrat, B. Teychene, Modification of tubular ceramic membranes with carbon nanotubes using catalytic chemical vapor deposition, Water Sci. Technol. 72 (2015) 1404–1410, https://doi.org/10.2166/ wst.2015.340.

[11] Z. Hu, Y. Yang, Q. Chang, F. Liu, Y. Wang, J. Rao, Preparation of a high- performance porous ceramic membrane by a two-step coating method and one-step sintering, Appl. Sci. 9 (2019) 52, https://doi.org/10.3390/app9010052.

[12] J. Yang, L. Yin, H. Tang, H. Song, X. Gao, K. Liang, C. Li, Polyelectrolyte- fluorosurfactant complex-based meshes with superhydrophilicity and superoleophobicity for oil/water separation, Chem. Eng. J. 268 (2015) 245–250, https://doi.org/10.1016/j.cej.2015.01.073.

[13] X. Zhu, A. Dudchenko, X. Gu, D. Jassby, Surfactant-stabilized oil separation from water using ultrafiltration and nanofiltration, J. Membr. Sci. 529 (2017) 159–169, https://doi.org/10.1016/j.memsci.2017.02.004.

[14] M. Matos, G. Guti´errez, A. Lobo, J. Coca, C. Pazos, J.M. Benito, Surfactant effect on the ultrafiltration of oil-in-water emulsions using ceramic membranes, J. Membr. Sci. 520 (2016) 749–759, https://doi.org/10.1016/j.memsci.2016.08.037.

[15] C. Li, W. Sun, Z. Lu, X. Ao, S. Li, Ceramic nanocomposite membranes and membrane fouling: a review, Water Res. 175 (2020), 115674, https://doi.org/10.1016/j.watres.2020.115674.

[16] D. Venegoni, P. Serp, R. Feurer, Y. Kihn, C. Vahlas, P. Kalck, Parametric study for the growth of carbon nanotubes by catalytic chemical vapor deposition in a fluidized bed reactor, Carbon 40 (2002) 1799–1807, https://doi.org/10.1016/ S0008-6223(02)00057-X.

[17] G.S.B. McKee, C.P. Deck, K.S. Vecchio, Dimensional control of multi-walled carbon nanotubes in floating-catalyst CVD synthesis, Carbon 47 (2009) 2085–2094, https://doi.org/10.1016/j.carbon.2009.03.060.

[18] J. Chen, Q. Chen, Q. Ma, Influence of surface functionalization via chemical oxidation on the properties of carbon nanotubes, J. Colloid Interface Sci. 370 (2012) 32–38, https://doi.org/10.1016/j.jcis.2011.12.073.

[19] B. Sarkar, S. Mandal, Y.F. Tsang, P. Kumar, K.-H. Kim, Y.S. Ok, Designer carbon nanotubes for contaminant removal in water and wastewater: a critical review, Sci. Total Environ. 612 (2018) 561–581, https://doi.org/10.1016/j.scitotenv.2017.08.132.

[20] V. Vatanpour, M. Esmaeili, M.H.D.A. Farahani, Fouling reduction and retention increment of polyethersulfone nanofiltration membranes embedded by amine-functionalized multi-walled carbon nanotubes, J. Membr. Sci. 466 (2014) 70–81, https://doi.org/10.1016/j.memsci.2014.04.031.

[21] J. Saththasivam, W. Yiming, K. Wang, J. Jin, Z. Liu, A novel architecture for carbon nanotube membranes towards fast and efficient oil/water separation, Sci. Rep. 8 (2018) 7418, https://doi.org/10.1038/s41598-018-25788-9.

[22] B. Roman-Manso, S.M. Vega-Diaz, A. Morelos-Gomez, M. Terrones, P. Miranzo, ´ M. Belmonte, Aligned carbon nanotube/silicon carbide hybrid materials with high electrical conductivity, superhydrophobicity and superoleophilicity, Carbon 80 (2014) 120–126, https://doi.org/10.1016/j.carbon.2014.08.046.

[23] T.J. Ainscough, P. Alagappan, D.L. Oatley-Radcliffe, A.R. Barron, A hybrid super hydrophilic ceramic membrane and carbon nanotube adsorption process for clean water production and heavy metal removal and recovery in remote locations, J. Water Process. Eng. 19 (2017) 220–230, https://doi.org/10.1016/j. jwpe.2017.08.006.

[24] S. Ali, S.A.U. Rehman, H.-Y. Luan, M.U. Farid, H. Huang, Challenges and opportunities in functional carbon nanotubes for membrane-based water treatment and desalination, Sci. Total Environ. 646 (2019) 1126–1139, https://doi.org/10.1016/j.scitotenv.2018.07.348.

[25] L. Bai, H. Liang, J. Crittenden, F. Qu, A. Ding, J. Ma, X. Du, S. Guo, G. Li, Surface modification of UF membranes with functionalized MWCNTs to control membrane fouling by NOM fractions, J. Membr. Sci. 492 (2015) 400–411, https://doi.org/10.1016/j.memsci.2015.06.006.

[26] Ihsanullah, Carbon nanotube membranes for water purification: developments, challenges, and prospects for the future, Sep. Purif. Technol. 209 (2019) 307–337, https://doi.org/10.1016/j.seppur.2018.07.043.

[27] D. Mattia, H. Leese, K.P. Lee, Carbon nanotube membranes: from flow enhancement to permeability, J. Membr. Sci. 475 (2015) 266–272, https://doi.org/10.1016/j.memsci.2014.10.035.

[28] M.H.-O. Rashid, S.F. Ralph, Carbon nanotube membranes: synthesis, Properties, and Future Filtration Applications, Nanomaterials. 7 (2017) 99, https://doi.org/10.3390/nano7050099.

[29] G.S. Ajmani, D. Goodwin, K. Marsh, D.H. Fairbrother, K.J. Schwab, J.G. Jacangelo, H. Huang, Modification of low pressure membranes with carbon nanotube layers for fouling control, Water Res. 46 (2012) 5645–5654, https://doi.org/10.1016/j.watres.2012.07.059.

[30] M. Sianipar, S. Hyun Kim, F. Khoiruddin, I.Gede Iskandar, Wenten, Functionalized carbon nanotube (CNT) membrane: progress and challenges, RSC Adv. 7 (2017) 51175–51198, https://doi.org/10.1039/C7RA08570B.

[31] X. Chen, L. Hong, Y. Xu, Z.W. Ong, Ceramic pore channels with inducted carbon nanotubes for removing oil from water, ACS Appl. Mater. Interfaces 4 (2012) 1909–1918, https://doi.org/10.1021/am300207b.

[32] K. Yuan, S. Feng, F. Zhang, Z. Zhong, W. Xing, Steric configuration-controllable carbon nanotubes-integrated SiC membrane for ultrafine particles filtration, Ind. Eng. Chem. Res. 59 (2020) 19680–19688, https://doi.org/10.1021/acs.iecr.0c03581.

[33] A.-C. Dupuis, The catalyst in the CCVD of carbon nanotubes—a review, Prog. Mater. Sci. 50 (2005) 929–961, https://doi.org/10.1016/j.pmatsci.2005.04.003.

[34] L. Jodin, A.-C. Dupuis, E. Rouvi`ere, P. Reiss, Influence of the catalyst type on the growth of carbon nanotubes via methane chemical vapor deposition, J. Phys. Chem. B 110 (2006) 7328–7333, https://doi.org/10.1021/jp056793z.

[35] K. Hernadi, Z. Konya, A. Siska, J. Kiss, A. Oszk´ o, J.B. Nagy, I. Kiricsi, On the role of ´ catalyst, catalyst support and their interaction in synthesis of carbon nanotubes by CCVD, Mater. Chem. Phys. 77 (2003) 536–541, https://doi.org/10.1016/S0254-0584(02)00105-0.

[36] E.F. Kukovitsky, S.G. L'vov, N.A. Sainov, V.A. Shustov, L.A. Chernozatonskii, Correlation between metal catalyst particle size and carbon nanotube growth, Chem. Phys. Lett. 355 (2002) 497–503, https://doi.org/10.1016/S0009-2614(02) 00283-X.

[37] S.B. Sinnott, R. Andrews, D. Qian, A.M. Rao, Z. Mao, E.C. Dickey, F. Derbyshire, Model of carbon nanotube growth through chemical vapor deposition, Chem. Phys. Lett. 315 (1999) 25–30, https://doi.org/10.1016/S0009-2614(99)01216-6.

[38] S.W. Chee, R. Sharma, Controlling the size and the activity of fe particles for synthesis of carbon nanotubes, Micron 43 (2012) 1181–1187, https://doi.org/10.1016/j.micron.2012.01.008.

[39] A.R. Harutyunyan, G. Chen, T.M. Paronyan, E.M. Pigos, O.A. Kuznetsov, K. Hewaparakrama, S.M. Kim, D. Zakharov, E.A. Stach, G.U. Sumanasekera, Preferential growth of single-walled carbon nanotubes with metallic conductivity, Science 326 (2009) 116–120, https://doi.org/10.1126/science.1177599.

[40] W.Z. Li, S.S. Xie, L.X. Qian, B.H. Chang, B.S. Zou, W.Y. Zhou, R.A. Zhao, G. Wang, Large-scale synthesis of aligned carbon nanotubes, Science 274 (1996) 1701–1703, https://doi.org/10.1126/science.274.5293.1701.

[41] S. Noda, K. Hasegawa, H. Sugime, K. Kakehi, Z. Zhang, S. Maruyama, Y. Yamaguchi, Millimeter-thick single-walled carbon nanotube forests: hidden role of catalyst support, Jpn. J. Appl. Phys. 46 (2007) L399, https://doi.org/10.1143/JJAP.46.L399.

[42] T. Tomie, S. Inoue, M. Kohno, Y. Matsumura, Prospective growth region for chemical vapor deposition synthesis of carbon nanotube on C-H–O ternary diagram, Diam. Relat. Mater. 19 (2010) 1401–1404, https://doi.org/10.1016/j. diamond.2010.08.005.

[43] M. He, Y. Magnin, H. Amara, H. Jiang, H. Cui, F. Fossard, A. Castan, E. Kauppinen, A. Loiseau, C. Bichara, Linking growth mode to lengths of single-walled carbon nanotubes, Carbon 113 (2017) 231–236, https://doi.org/10.1016/j.carbon.2016.11.057.

[44] A. Botello-M´endez, J. Campos-Delgado, A. Morelos-Gomez, J.M. Romo-Herrera, ´ A. G. Rodríguez, H. Navarro, M.A. Vidal, H. Terrones, M. Terrones, Controlling the dimensions, reactivity and crystallinity of multiwalled carbon nanotubes using low ethanol concentrations, Chem. Phys. Lett. 453 (2008) 55–61, https://doi.org/10.1016/j.cplett.2007.12.073.

[45] G. Gulino, R. Vieira, J. Amadou, P. Nguyen, M.J. Ledoux, S. Galvagno, G. Centi, C. Pham-Huu, C2H6 as an active carbon source for a large scale synthesis of carbon nanotubes by chemical vapour deposition, Appl. Catal. A Gen. 279 (2005) 89–97, https://doi.org/10.1016/j.apcata.2004.10.016.

[46] C.J. Lee, J. Park, Y. Huh, J., Yong lee, temperature effect on the growth of carbon nanotubes using thermal chemical vapor deposition, Chem. Phys. Lett. 343 (2001) 33–38, https://doi.org/10.1016/S0009-2614(01)00680-7.

[47] C.-S. Kuo, A. Bai, C.-M. Huang, Y.-Y. Li, C.-C. Hu, C.-C. Chen, Diameter control of multiwalled carbon nanotubes using experimental strategies, Carbon 43 (2005) 2760–2768, https://doi.org/10.1016/j.carbon.2005.05.022.

[48] C. Hoecker, F. Smail, M. Pick, A. Boies, The influence of carbon source and catalyst nanoparticles on CVD synthesis of CNT aerogel, Chem. Eng. J. 314 (2017) 388–395, https://doi.org/10.1016/j.cej.2016.11.157.

[49] M. Monthioux, P. Serp, E. Flahaut, M. Razafinimanana, C. Laurent, A. Peigney, W. Bacsa, J.-M. Broto, Introduction to carbon nanotubes, in: Springer Handbook of Nanotechnology, Springer, Berlin, Heidelberg, 2010, pp. 47–118, https://doi.org/10.1007/978-3-642-02525-9_3.

[50] E.F. Antunes, A.O. Lobo, E.J. Corat, V.J. Trava-Airoldi, Influence of diameter in the raman spectra of aligned multi-walled carbon nanotubes, Carbon 45 (2007) 913–921, https://doi.org/10.1016/j.carbon.2007.01.003.

[51] L. Vanyorek, D. Loche, H. Katona, M.F. Casula, A. Corrias, Z. Konya, ´ A. Kukovecz, ´ I. Kiricsi, Optimization of the catalytic chemical vapor deposition synthesis of multiwall carbon nanotubes on FeCo(Ni)/SiO2 aerogel catalysts by statistical design of experiments, J. Phys. Chem. C 115 (2011) 5894–5902, https://doi.org/10.1021/jp111860x.

[52] T.W. Hansen, A.T. DeLaRiva, S.R. Challa, A.K. Datye, Sintering of catalytic nanoparticles: particle migration or Ostwald ripening? Acc. Chem. Res. 46 (2013) 1720–1730, https://doi.org/10.1021/ar3002427.

[53] S.V. Bulyarskiy, G.G. Gusarov, A.V. Lakalin, M.S. Molodenskiy, A.A. Pavlov, R. M. Ryazanov, Vertically aligned carbon nanotube arrays growth modeling at different temperatures and pressures in reactor, Diam. Relat. Mater. 103 (2020), 107665, https://doi.org/10.1016/j.diamond.2019.107665.

[54] A. Nourbakhsh, B. Ganjipour, M. Zahedifar, E. Arzi, Morphology optimization of CCVD-synthesized multiwall carbon nanotubes, using statistical design of experiments, Nanotechnology 18 (2007), 115715, https://doi.org/10.1088/0957- 4484/18/11/115715.

[55] R. Vieira, C. Pham-Huu, N. Keller, M.J. Ledoux, New carbon nanofiber/graphite felt composite for use as a catalyst support for hydrazine catalytic decomposition, Chem. Commun. 954 (2002).

[56] L.S.K. Pang, J.D. Saxby, S.P. Chatfield, Thermogravimetric analysis of carbon nanotubes and nanoparticles, J. Phys. Chem. 97 (1993) 6941–6942, https://doi.org/10.1021/j100129a001.

[57] A. Merlen, J.G. Buijnsters, C. Pardanaud, A guide to and review of the use of multiwavelength Raman spectroscopy for characterizing defective aromatic carbon solids: from graphene to amorphous carbons, Coatings 7 (2017) 153, https://doi.org/10.3390/coatings7100153.

[58] J. Goupy, L. Creighton, Introduction aux plans d'experiences, Dunod, Paris, 200´ 6.

[59] C. Lu, J. Liu, Controlling the diameter of carbon nanotubes in chemical vapor deposition method by carbon feeding, J. Phys. Chem. B 110 (2006) 20254–20257, https://doi.org/10.1021/jp0632283.

[60] R.V. Lenth, Quick and easy analysis of unreplicated factorials, Technometrics 31 (1989) 469–473, https://doi.org/10.1080/00401706.1989.10488595.

[61] R Development Core Team, R: A Language and Environment for Statistical Computing, R Foundation for Statistical Computing, Vienna, Austria, 2008.

[62] U. Gromping, R package FrF2 for creating and analyzing fractionnal factorial 2- level designs, J. Stat. Softw. 56 (2014) 1–56.

[63] S. Xie, G.-Q. Jin, S. Meng, Y.-W. Wang, Y. Qin, X.-Y. Guo, Microwave absorption properties of in situ grown CNTs/SiC composites, J. Alloys Compd. 520 (2012) 295–300, https://doi.org/10.1016/j.jallcom.2012.01.050.

[64] I. Polaert, S. Bastien, B. Legras, L. Estel, N. Braidy, Dielectric and magnetic properties of NiFe2O4 at 2.45GHz and heating capacity for potential uses under microwaves, J. Magn. Magn. Mater. 374 (2015) 731–739, https://doi.org/ 10.1016/j.jmmm.2014.09.027.

[65] A. de la Hoz, A. Loupy, Microwaves in Organic Synthesis, John Wiley & Sons, 2013.

[66] J. Ding, Q. Zhong, S. Zhang, Catalytic efficiency of iron oxides in decomposition of H2O2 for simultaneous NOX and SO2 removal: effect of calcination temperature, J. Mol. Catal. A Chem. 393 (2014) 222–231, https://doi.org/10.1016/j. molcata.2014.06.018.

[67] A. Sadezky, H. Muckenhuber, H. Grothe, R. Niessner, U. Poschl, Raman ¨ microspectroscopy of soot and related carbonaceous materials: spectral analysis and structural information, Carbon 43 (2005) 1731–1742, https://doi.org/10.1016/j.carbon.2005.02.018.

[68] P. Vinten, J. Lefebvre, P. Finnie, Kinetic critical temperature and optimized chemical vapor deposition growth of carbon nanotubes, Chem. Phys. Lett. 469 (2009) 293–297, https://doi.org/10.1016/j.cplett.2008.12.095.

[69] A.C. Ferrari, J.C. Meyer, V. Scardaci, C. Casiraghi, M. Lazzeri, F. Mauri, S. Piscanec, D. Jiang, K.S. Novoselov, S. Roth, A.K. Geim, Raman spectrum of graphene and graphene layers, Phys. Rev. Lett. 97 (2006), 187401.

[70] C. Badre, Etude de la reactivit´ ´e de surface par mesure d'angle de contact: influence de la fonctionnalisation et de la structure: applications aux films d'oxyde de zinc electrod´ ´epos´es, These de doctorat, Paris 6, 2007, ` https://www.theses.fr/2007PA0 66282. (Accessed 28 January 2021).

[71] J. Zheng, S. Xu, Z. Wu, Z. Wang, Removal of p-chloroaniline from polluted waters using a cathodic electrochemical ceramic membrane reactor, Sep. Purif. Technol. 211 (2019) 753–763, https://doi.org/10.1016/j.seppur.2018.10.046.

[72] K. Wei, T. Cui, F. Huang, Y. Zhang, W. Han, Membrane separation coupled with electrochemical advanced oxidation processes for organic wastewater treatment: a short review, Membranes. 10 (2020) 337, https://doi.org/10.3390/membranes10110337.

[73] T.X. Huong Le, L.F. Dum´ee, S. Lacour, M. Rivallin, Z. Yi, L. Kong, M. Bechelany, M. Cretin, Hybrid graphene-decorated metal hollow fibre membrane reactors for efficient electro-Fenton - filtration co-processes, J. Membr. Sci. 587 (2019), 117182, https://doi.org/10.1016/j.memsci.2019.117182.

[74] B. Lanfant, Y. Leconte, N. Debski, G. Bonnefont, M. Pinault, M. Mayne-L'Hermite, A. Habert, Y. Jorand, V. Garnier, G. Fantozzi, S. Le Gallet, F. Bernard, Mechanical, thermal and electrical properties of nanostructured CNTs/SiC composites, Ceram. Int. 45 (2019) 2566–2575, https://doi.org/10.1016/j.ceramint.2018.10.187.

[75] W. Fu, W. Zhang, Microwave-enhanced membrane filtration for water treatment, J. Membr. Sci. 568 (2018) 97–104, https://doi.org/10.1016/j.memsci.2018.09.064.

[76] N. Benamara, Intensification de proc´edes par chauffage micro-ondes pour la chimie´ verte, Normandie Universit´e, 2017.

[77] M. Fortuny, C.B.Z. Oliveira, R.L.F.V. Melo, M. Nele, R.C.C. Coutinho, A.F. Santos, Effect of salinity, temperature, water content, and pH on the microwave demulsification of crude oil emulsions, Energy Fuel 21 (2007) 1358–1364, https:// doi.org/10.1021/ef0603885.